https://doi.org/10.1016/j.conbuildmat.2021.124275

Energy-Based Characterization of the Fatigue Crack Density Evolution of Asphalt Binders Through Controlled-Stress Fatigue Testing

Chenguang Shi, Ph.D. Candidate
School of Transportation, Southeast University
#2 Southeast University Road, Nanjing, 211189, PR China
Email: chenguangshi@seu.edu.cn

Xing Cai, Ph.D. Candidate
School of Transportation, Southeast University
#2 Southeast University Road, Nanjing, 211189, PR China
Email: tsing2017@seu.edu.cn

Tianling Wang, Master Candidate
School of Transportation, Southeast University
#2 Southeast University Road, Nanjing, 211189, PR China
Email: wangtianling@seu.edu.cn

Xingyu Yi, Ph.D. Candidate
School of Transportation, Southeast University
#2 Southeast University Road, Nanjing, 211189, PR China
Email: yixingyu@seu.edu.cn

Song Liu, Ph.D.
College of Civil Engineering, Nanjing Forestry University
159 Longpan Road, Nanjing, Jiangsu, 210037, PR China
Email: ls2020@njfu.edu.cn

Jun Yang, Ph.D., Professor
(Corresponding Author)
School of Transportation, Southeast University
#2 Southeast University Road, Nanjing, 211189, PR China
Email: yangjun@seu.edu.cn

Zhen Leng, Ph.D., Associate Professor
Department of Civil and Environmental Engineering, The Hong Kong Polytechnic University
Hong Kong, 999077, China
Email: zhen.leng@polyu.edu.hk

Abstract

Fatigue crack behavior of asphalt binder plays an important influence on the fatigue performance of asphalt pavements. To evaluate the fatigue crack density evolution within the steady growth stage of #70 unmodified asphalt binder and SBS modified asphalt binder, the crack initiation and propagation were characterized based on Griffith theory and modified Paris' law, respectively. Aiming to calculate the horizontal length of crack initiation (a), the surface free energy of those two asphalt binders were calculated by contact angle measured with Wilhelmy plate test. Also, the stress sweep tests and time sweep tests were performed using Dynamic Shear Rheometer (DSR) to obtain the mechanical parameters of asphalt binders for calculation of fatigue crack density (ϕ) and dissipated pseudo strain energy (DPSE). They were fitted by modified Paris' law, and coefficients n and A were determined. Results show that a for two asphalt binders increase with the increasing stress level and SBS modified asphalt binder shows a larger crack size in crack initiation, which means that SBS modified asphalt binder shows a better crack initiation resistance compared with unmodified asphalt binder. The ϕ and DPSE within the steady growth stage follow the linear relationship, indicating that the unit DPSE causes the equal amount of increase in ϕ. In addition, the A and n are independent on the stress levels. They are fundamental material properties and there is a linear relationship between the log(A) and n. SBS modified asphalt binder processes the better fatigue crack resistance because of the smaller value of n.

Keywords:

Asphalt binder, Fatigue crack density, Crack initiation, Crack propagation, Surface free energy, Modified Paris' law

1. Introduction

Fatigue crack is a common type of damage that occurs in asphalt pavement. There are two types of fatigue cracks: cohesive cracks (occurring within an asphalt binder) and adhesive cracks (occurring at the asphalt binder-aggregate interface) [1]. As an important component of asphalt mixture, the fatigue crack resistance of asphalt binder determines its fatigue performance [2-3]. Therefore, the evaluation of asphalt binder fatigue crack resistance has been one of the most popular topics of asphalt materials to date.

Under repeated loading, the fatigue process of asphalt binder experiences three distinct stages: crack initiation, steady crack propagation, and unsteady crack propagation. The photographic technique is an effective way to visualize the crack length of an asphalt binder sample under different loading cycles, and related studies have shown that circumferential hairline cracks generated at the periphery of a sample (crack initiation) and propagated inward (crack propagation), resulting in a decrease of the effective sample radius [1, 4]. In order to understand the evolution of fatigue cracks and accurately evaluate the damage degree of an asphalt binder sample, the crack length of formulation has been derived from the stress and strain [1, 5-6] or developed according to damage mechanics principles [7-9]. At the beginning of a fatigue test, the fatigue crack damage degree shows a sharp increase due to molecular rearrangements [10-11], microcrack nucleation [12], and circumferential crack formation [5, 7]. When the crack formation is complete, the fatigue crack damage degree will show a steady increase. Therefore, the onset of the steady growth stage is the crack initiation [13]. Once the asphalt binder loses the ability of crack resistance, the fatigue damage degree will dramatically increase, e.g., stepping into the unsteady growth stage. Normally, the steady growth stage attracts the attention of more researchers because it represents the fatigue crack resistance of an asphalt binder to a large extent.

Crack initiation is the premise of propagation [14], which is critical for evaluating crack propagation. Therefore, crack initiation needs to be analyzed first. In order to figure out the crack initiation mechanism, some pioneers have developed local crack growth criteria for viscoelastic materials to solve the problems related to crack initiation. Based on continuum mechanics, Knauss [15] developed a crack speed criterion. Schapery [16] proposed a crack tip model and a local energy criterion for evaluating crack initiation. However, those two theories were too complex to apply to engineering practice because the description of crack initiation using the theories involves numerous details [14]. To circumvent this limitation, Griffith's energy criterion has been used to

deal with the crack initiation of asphalt materials. In this theory, the potential energy of the asphalt material body is regarded as a balanced station when cracks are initiated. Following this theory, the crack initiation criteria of asphalt mixture under tensile loading and compressive loading were developed [14, 17]. Moreover, the crack initiation of an asphalt binder under rotational shear loading was successfully analyzed based on the Griffith's energy criterion [13]. Particularly, Li et al. [18] employed this theory to investigate the crack initiation of waste-derived asphalt binders (e.g., bio-oil modified asphalt and plastic modified asphalt using polyethylene). In this study, Griffith's energy criterion was applied to study the crack initiation length of asphalt binders under different stress levels.

To characterize crack propagation, Paris' law is commonly used to build the relationship between the fatigue crack growth rate and the pseudo strain energy release rate [8, 19-23]. According to the fitting of the test results with Paris' law, the parameters A and n are obtained to evaluate the fatigue crack performance of asphalt materials. Normally, Paris' law is applied to model the damage growth of a single crack for asphalt mixture [19-20] and for asphalt binder [8, 18, 21-22]. However, Paris' law has made the accuracy of crack propagation evaluation for asphalt materials pale because there are a multitude of cracks propagating in asphalt materials under cyclic loading. To address this problem, Si et al. [24] proposed that the crack length of a single crack could be replaced by the damage density, e.g., the ratio of area of all cracks to the total area of a sample, to evaluate the fatigue crack growth of asphalt mixtures. Later, the concept of damage crack density was successfully employed in a modified Paris' law to characterize the fracture resistance of asphalt mixture [25-28]. Therefore, the fatigue crack density of an asphalt binder proposed by authors will be employed in characterizing the fatigue crack evolution in this study [9]. Another important part of Paris' law is the pseudo strain energy release rate, which was proposed by Schapery [29] to replace the stress intensity factor due to the viscoelastic characterization of asphalt binder. Usually, the total dissipated pseudo strain energy is used to determine the pseudo strain energy release rate. However, the energy is used not only for cracking but also used for other behaviors, such as permanent deformation and the viscoelastic effect [20].

Consequently, in this study, in order to understand the fatigue crack evolution behavior of two types of asphalt binders under controlled-stress loading, including #70 unmodified asphalt binder and SBS modified asphalt binder, the crack initiation and propagation in the steady growth stage whose range was determined by the secant method were analyzed simultaneously for various

stress levels. To accurately evaluate the fatigue crack growth rate, only the dissipated pseudo strain energy due to fatigue cracking was applied in the calculation of the pseudo strain energy release rate. Therefore, this paper is organized as follows. First, the materials and the laboratory tests, including the DSR test and the Wilhelmy plate test for contact angle measurement, are described. The subsequent section describes the background and the theory containing the analysis of the fatigue crack density growth stages, crack initiation analysis based on the Griffith theory, and fatigue crack density propagation using the modified Paris' law. Then the corresponding discussions of the horizontal length of the crack initiation, the relationship between the fatigue crack density and the dissipated pseudo strain energy for cracking, and the modified Paris' law parameters related to crack growth rate are presented. The last section concludes the paper with the main contributions of this study.

2. Materials and Laboratory Tests

2.1. Materials

Herein, two kinds of asphalt binders commonly used in China were studied, including #70 unmodified asphalt binder and SBS modified asphalt binder whose content of SBS polymer of the control binder was 4% by weight. The basic properties of the asphalt binders, including penetration, softening point, and ductility, were tested based on the methods in the specification JTG E20-2011 [30], as listed in Table 1. The results met the requirements in the specification JTG F40-2004 [31]. These two asphalt binders were prepared as DSR tests samples and Wilhelmy plate test specimens, which were used to measure the viscoelastic mechanical parameters and contact angles for the calculation of the surface energies of the asphalt binders.

Table 1 Basic properties of asphalt binders

Asphalt type	Penetration (25℃, 100 g, 5 s)/0.1 mm	Ductility (10℃, 5 cm/min)/ cm	Softening point/℃
#70	68.5	50.0	47.0
SBS	53.0	＞100	94.5

2.2. DSR tests

To obtain the viscoelastic mechanical parameters of asphalt binders, the asphalt binder samples were subjected to DSR tests with a parallel plate of 8 mm having a gap of 2 mm [32]. First, the samples were subjected to stress sweep tests in which the amplitude of shear stress increased logarithmically from 0.1 kPa to 400 kPa without any rest periods in order to find the

critical point of the stress level between the undamaged stage and the damage stage, which played an important role in determining the stress levels for the time sweep tests. The critical points of the stress level for the #70 unmodified asphalt binder and the SBS modified asphalt binder were 150.2 kPa and 157.4 kPa, respectively. Furthermore, the linear viscoelastic (undamaged stage) mechanical parameters obtained from the stress sweep tests were of great significance in analyzing the behaviors of the fatigue crack density propagation. The average values of the phase angle and the dynamic shear modulus within the undamaged stage for those two asphalt binders were 56.5°, 6583.9 kPa and 53.4°, 5588.4 kPa. Second, the time sweep tests at high stress levels (180 kPa, 200 kPa, 220 kPa, 240 kPa, 260 kPa, 280 kPa, and 300 kPa) were conducted for each tested sample under controlled-stress rotational shear loading. All of the tests were performed at 20°C and 10 Hz, with two replicates for every testing condition.

2.3. Wilhelmy plate test for the calculation of the surface free energy (SFE)

The Wilhelmy plate method is a common way to measure the contact angles between asphalt binders and liquids. The testing data were used to calculate the SFE components of the asphalt binders based on the Young-Dupre equation (see Eq. (1)) [33]. As shown in Eq. (1), the calculation of SFE components of the asphalt binders required the measurement of the contact angles between the asphalt binders and at least three probe liquids with known surface energy components. In this study, probe liquids (glycerol, ethylene glycol, formamide, and distilled water) with various polarities were selected. The surface free energy components of these four probe liquids are shown in Table 2. In order to obtain the contact angle, glass plate specimens coated with a thin asphalt film were immersed in the liquids mentioned above at a constant rate of 3 mm/min and 20°C, which was coincident with DSR tests. During this process, the force applied to the specimen was constantly recorded. Then the contact angle between the asphalt binders and the liquids could be calculated with a kinetic force balance [34]. Three replicates were measured for every type of probe liquid. Three replicates were measured for every type of probe liquid, and the average values of contact angle were shown in Table 3.

$$[1+\cos\theta]\Gamma_L = 2\left(\sqrt{\Gamma_S^-\Gamma_L^+} + \sqrt{\Gamma_S^+\Gamma_L^-} + \sqrt{\Gamma_S^{LW}\Gamma_L^{LW}}\right) \quad (1)$$

where Γ is the surface free energy, mJ/m^2, the “S” subscript indicates the asphalt binders in this study, and the “L” subscript indicates the probe liquids. The “-” superscript indicates the Lewis base component, the “+” superscript indicates the Lewis acid component, and the “LW” superscript

indicates the Lifshitz-van der Waals component. θ is the contact angle between the asphalt binder sample and the probe liquid.

Once the SFE components of the asphalt binders were calculated, the total SFE of the asphalt binders could be determined based on the Good-van Oss-Chaudhury (GvOC) theory, as shown in Eq. (2) [35].

$$\Gamma = \Gamma^{LW} + \Gamma^{AB} = \Gamma^{LW} + 2\sqrt{\Gamma^{+}\Gamma^{-}}\,, \tag{2}$$

where the "AB" superscript indicates the Lewis polar acid-base component.

Table 2 Surface energy components of four known liquids at 20°C (mJ/m^2).

Known liquid	Γ^{LW}	Γ^{+}	Γ^{-}	Γ^{AB}	Γ
Glycerol	34.00	3.92	57.40	30.00	64.00
Ethylene Glycol	29.00	1.92	47.00	19.00	48.00
Formamide	39.00	2.28	39.60	19.00	58.00
Distilled Water	21.80	25.50	25.50	51.00	72.80

Table 3 Determined contact angles of asphalt binders with known liquids at 20 ℃.

Asphalt binder	Distilled Water		Formamide		Glycerol		Ethylene Glycol	
	Average/ °	CV/%	Average/ °	CV/%	Average/ °	CV/%	Average/ °	CV/%
#70	103.64	0.89	86.40	1.90	92.34	0.64	78.73	0.52
SBS	97.26	0.56	77.14	2.61	82.90	3.11	61.75	3.47

3. Background and Theory

3.1. Fatigue crack density growth stages

Under a periodic rotational shear load, the fatigue crack damage would extend from the edge of the cylindrical asphalt binder DSR sample to the center of the sample. In order to quantitatively analyze the fatigue crack of the asphalt binder, the fatigue crack density were proposed by authors [9]. The fatigue crack density was calculated by the ratios of the damaged volume to the total volume of the asphalt binder sample, shown in Eq. (3). In the DSR tests, the height of asphalt binder sample is invariable. Therefore, the fatigue crack density only changes with the decrease of effective radius of undamaged sample. In order to determine the effective radius, the torque equilibrium principle and dissipated strain energy (DSE) equilibrium principle were applied [9]. As shown in Eq. (4), the effective radius was calculated using mechanical parameters (dynamic shear modulus and phase angle) of asphalt binder on undamaged and damaged conditions. Fig. 1 shows a typical fatigue crack density curve with the increase of the load cycles for the controlled-stress fatigue testing. It was clear that the fatigue crack density of

the asphalt binder experienced three stages, i.e., the crack initiation stage (Stage I), steady growth stage (Stage II), and unsteady growth stage (Stage III). The fatigue crack density increased sharply with the shorter loading cycles within the Stage I, and the crack initiation finished at the end of this stage. Once the circumferential crack formed, the fatigue crack behavior of the asphalt binder stepped into steady growth stage, showing a linear increase of the fatigue crack density. Therefore, the onset of stage II was defined as the crack initiation. When the fatigue crack damage propagated to a higher level, the asphalt binder lost the ability of fatigue resistance, presenting a vertical increase in the fatigue crack density. Usually, researchers pay more attention to the mechanical behaviors within a steady growth stage because it undergoes more than 50% of the load cycles during the whole fatigue process.

$$\phi = \frac{V_{C,N}}{V_0} = \left(1 - \frac{\bar{V}}{V_0}\right) \times 100\% = \left(1 - \frac{\pi r_{E,N\text{th}}^2 h}{\pi r_0^2 h}\right) \times 100\% = \left(1 - \frac{r_{E,N\text{th}}^2}{r_0^2}\right) \times 100\% \quad , \tag{3}$$

Where $V_{C,N}$ is the cracked volume of the asphalt binder sample; $\bar{V}$ is the undamaged volume of the asphalt binder sample; V_0 is the total volume of the asphalt binder sample; $r_{E,N\text{th}}$ is the effective radius of undamaged part at the *N*th load cycle, which was determined with Eq. (4), in mm, r_0 is the initial radius of the sample, $r_0 = 4mm$, and *h* is the height of the sample, $h = 2mm$.

$$r_{E,N\text{th}} = \left(\frac{\left|G_{NF}^*\right|}{\left|G_{VE}^*\right|} \cdot \frac{\sin\delta_{VE}}{\sin\delta_{NF}}\right)^{0.25} \cdot r_0 \, , \tag{4}$$

where $\left|G_{VE}^*\right|$ and $\left|G_{NF}^*\right|$ are the dynamic shear modulus of the undamaged condition and the *N*th fatigue loading cycle, respectively, in kPa, and δ_{VE} and δ_{NF} are the phase angles of the undamaged and *N*th fatigue loading cycles, respectively, in radians.

However, the most difficult issue was the partitioning of the range of these three fatigue crack density growth stages. To resolve this problem, the secant method was performed to locate the critical points (the red points in Fig. 1) of the fatigue crack density between the different stages based on the concavity and convexity characteristics of the fatigue crack density curve [9]. The onset point of Stage III was the point where the slope of the secant line (the value of k_1), as shown

in Fig. 2(a) was at a minimum. Similarly, the demarcation point between Stage I and II was determined when the slope of the secant line (the value of k_2) was at a minimum with a reverse chronological order in the load cycles, as shown in Fig. 2(b). As a result, the range of Stage II was obtained.

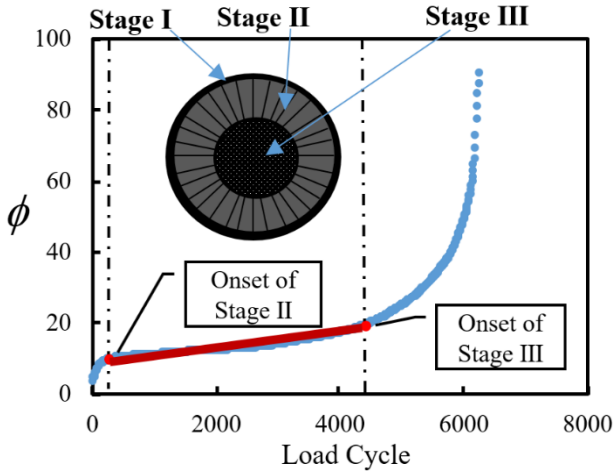

Fig. 1 Fatigue crack density growth trend with controlled-stress loading [9].

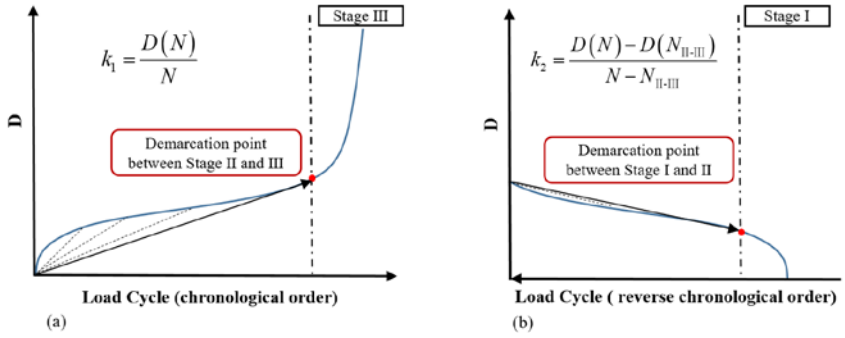

Fig. 2 Partition of the fatigue crack density curve based on the secant method: (a) determination of the demarcation point between Stage II and III, and (b) determination of demarcation point between Stage I and II [9].

The fatigue crack damage was a process of energy redistribution within the asphalt binder sample based on the Griffith theory [13]. There were two types of energies (recoverable pseudo strain energy [RPSE] and dissipated pseudo strain energy [DPSE]) that were generated during the fatigue testing with sinusoidal unloading and loading, as shown in Fig. 3 [36]. The RPSE was equal to the area between the stress-pseudo strain curve and the horizontal axis, which was stored and recovered corresponding to the purely elastic effect of the material [13, 37]. The RPSE played an important role in the analysis of the crack initiation. The DPSE was equal to the area of the stress-pseudo strain loop, representing the energy dissipated in a loading cycle due to

damage [37-38]. Therefore, the DPSE was suitable for depicting the fatigue crack behavior of the asphalt binder during the fatigue testing. Detailed information about the energies is provided in section 3.2 and section 3.3. Likewise, the energy-based characterization of the fatigue crack density evolution within the steady growth stage was also the main research subject in this study.

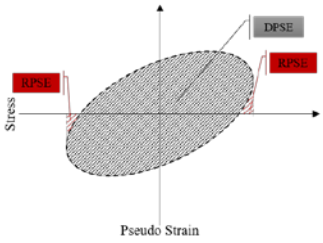

Fig. 3 Illustration of energy components: dissipated pseudo strain energy (DPSE) and recoverable pseudo strain energy (RPSE) [36].

3.2. Crack initiation analysis based on Griffith theory

Under the sinusoidal stress loading, the applied stress and strain response could be described using Eq. (5) and Eq. (6).

$$\tau = \tau_{0F} \sin\left(\omega t\right) \tag{5}$$

$$\gamma = \gamma_{0NF} \sin\left(\omega t - \delta_{NF}\right) \tag{6}$$

where τ_{0F}, γ_{0NF}, and δ_{NF} are the stress amplitude, strain amplitude, and phase angle of the damaged condition, respectively, ω is the angular frequency, and t is the loading time.

The corresponding pseudo strain for the controlled-stress mode had the form shown in Eq. (7).

$$\gamma^R = \gamma_0^R \sin\left(\omega t - \delta_{NF} + \delta_{VE}\right) = \frac{G_{VE}^*}{G_R} \gamma_{0NF} \sin\left(\omega t - \delta_{NF} + \delta_{VE}\right) \tag{7}$$

where γ_0^R is the pseudo strain amplitude, δ_{VE} is the phase angle within the linear viscoelastic stage, and G_{VE}^* and G_R are the dynamic shear modulus within the linear viscoelastic stage and the reference modulus, which were equal in this study.

According to the definition of the RPSE, the value of the RPSE density at a given radial position was determined with the function shown in Eq. (8) [13].

$$RPSE\left(r\right) = \frac{1}{2} \tau_{0F} \gamma_0^R = \frac{1}{2} \frac{\left(G_{VE}^* \theta r\right)^2}{G_R h^2}, \tag{8}$$

where the θ is the rotational angle.

As analyzed above, the crack initiation was the point where the steady growth stage started, so Eq. (8) was rewritten as shown in Eq. (9).

$$RPSE\left(c_0\right)=\frac{1}{2}\tau_{0F}\gamma_0^R=\frac{1}{2}\frac{\left(G_{VE}^*\theta\right)^2}{G_R h^2}\cdot\left(r_0-c_0\right)^2, \tag{9}$$

where the c_0 is the crack length of Stage I, which was determined with Eq. (10).

$$c_0=r_0-r_E \tag{10}$$

where the r_E is effective radius of the asphalt binder sample.

Based on the Griffith theory, the energy-based crack initiation criteria of the asphalt binder sample for the time sweep test were proposed, which could be described using Eq. (11) [13].

$$RPSE\left(r\right)\cdot k\cdot a\cdot\left(r_0-c_0\right)-2\Gamma\cdot\left(r_0-c_0-a\right)=0, \tag{11}$$

where *a* is the horizontal length of the crack initiation and *k* is the coefficient of the vertical height, which was determined to be 2π [39], as shown in Fig. 4.

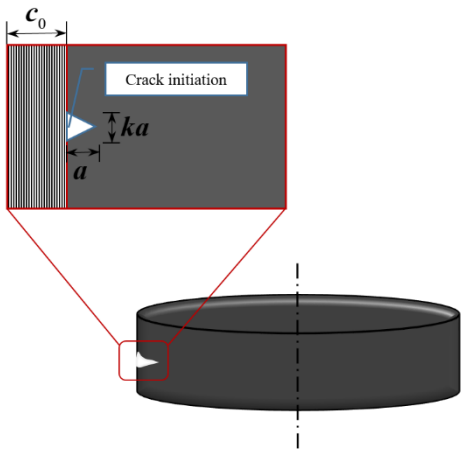

Fig. 4 The cracking initiation pattern of the asphalt binder DSR sample under fatigue testing. c_0 is the crack size of Stage I, a is the crack length of the crack initiation, and k the is the coefficient of the vertical height [13].

In order to simplify the formulation of Eq. (11), r_0-c_0-a was replaced by r_0-c_0 due to $a\ll c_0$. After substituting Eq. (9) into Eq. (11), the relationship between the SFE of the asphalt binder and the model parameters of the crack initiation gave

286 $$\Gamma = \frac{1}{4}\frac{\left(G_{VE}^{*}\theta\right)^{2}}{G_{R}h^{2}} \cdot \left(r_{0} - c_{0}\right)^{2} ka \tag{12}$$

287 *3.3. Fatigue crack density propagation analysis based on the DPSE with the modified Paris' law*

288 For controlled-stress loading, the DPSE could be represented by Eq. (13).

289 $$\begin{aligned} DPSE &= \pi\tau_{0F}\gamma_{0}^{R}\sin\left(\delta_{NF} - \delta_{VE}\right) \\ &= \pi\frac{\tau_{0F}^{2}}{G_{NF}^{*}}\sin\left(\delta_{NF} - \delta_{VE}\right) \end{aligned}, \tag{13}$$

290 where G_{NF}^{*} is the dynamic shear modulus within the damaged stage.

291 During the fatigue testing process, permanent deformation and cracking are common
292 distresses for an asphalt binder and they occur simultaneously. Therefore, the dissipated energy
293 could be divided into several components because of diverse damage effects. Masad [20] modified
294 Eq. (13) into Eq. (14) considering the following three components: (1) viscoelastic energy (W_{R1},
295 see Eq. [15]) for the change of the phase angle, (2) permanent deformation (W_{R2}, see Eq. [17]),
296 and (3) cracking (W_{R3} see Eq. [16]). Eq. (13) was multiplied by (G_{NF}^{*}/G_{VE}^{*}) to calculate the W_{R1},
297 which was the dissipated energy at the reference undamaged dynamic shear modulus. The W_{R3}
298 was related to the difference of the dynamic shear modulus between the undamaged condition and
299 the damaged condition.

300 $$DPSE = W_{R1} + W_{R2} + W_{R3} \tag{14}$$

301 $$W_{R1} = \frac{G_{NF}^{*}}{G_{VE}^{*}}DPSE = \pi\frac{\tau_{0F}^{2}}{G_{VE}^{*}}\sin\left(\delta_{NF} - \delta_{VE}\right) \tag{15}$$

302 $$W_{R3} = \frac{1}{2}\tau_{0F}\left(\gamma_{0NF}^{R} - \gamma_{0VE}^{R}\right) = \frac{1}{2}\tau_{0F}^{2}\left(\frac{1}{G_{NF}^{*}} - \frac{1}{G_{VE}^{*}}\right) \tag{16}$$

303 $$W_{R2} = DPSE - W_{R1} - W_{R3} \tag{17}$$

304 As a viscoelastic material, the evolution speed of the damage type of an asphalt binder is
305 determined by the testing temperature. In this study, the main distress of the asphalt binder samples
306 was cracking because of the lower temperature (20°C). Therefore, the dissipated energy calculated
307 with Eq. (16) was used to analyze the fatigue crack density evolution.

308 Paris' law was proposed to describe the relationship between the crack growth rate of a

single crack and the stress intensity or J-integral [40]. For the asphalt materials, the pseudo J-integral Paris' law was modified by replacing the stress intensity or J-integral with the pseudo J-integral, as shown in Eq. (18).

$$\frac{\mathrm{d}c}{\mathrm{d}N} = A\left(\triangle J_R\right)^n, \tag{18}$$

where c is the crack size, N represents the loading cycles, A and n are the fitting parameters, and $\triangle J_R$ is the pseudo J-integral.

Paris' law was suitable for modeling the crack growth rate of a single crack. However, there were numerous cracks that propagated and merged within the asphalt material during the fatigue testing, resulting in the loss of the bearing area. In order to circumvent this limitation, a modified Paris' law (see Eq. [19]) was proposed using the damage density (ϕ), which was the ratio of the lost area to the total area of the sample [25].

$$\frac{\mathrm{d}\phi}{\mathrm{d}N} = A\left(\triangle J_R\right)^n, \tag{19}$$

where $\triangle J_R$ is the pseudo J-integral, representing the pseudo strain energy release rate per unit of cracking areas. $\triangle J_R$ was defined as shown in Eq. (20).

$$\triangle J_R = \frac{\partial DPSE}{\partial V_C} = \frac{\partial DPSE / \partial N}{\partial V_C / \partial N} = \frac{DPSE_N}{V_{C,N}}, \tag{20}$$

where $DPSE_N$ is the dissipated pseudo strain energy at the Nth loading cycle. As discussed above, this study only considers the $DPSE$ for cracking, so $DPSE_N$ in Eq. (20) is replaced by Eq. (21). And $V_{C,N}$ is the cracked volume of the asphalt binder sample, which was determined based on Eq. (22).

$$\begin{aligned} W_{R3,N} &= \iiint_{V_{\triangle C}} W_{R3,N}\left(r\right)\mathrm{d}V_{\triangle C} \approx W_{R3,N}\left(r\right)\cdot V_{\triangle C} \\ &= \frac{1}{2}\tau_{0F}^2\left(\frac{1}{G_{NF}^*} - \frac{1}{G_{VE}^*}\right)\cdot \pi h \cdot \left(\triangle c^2 + 2r_E \triangle c\right) \end{aligned}, \tag{21}$$

where $\triangle c$ is the increase of the crack size at the Nth loading cycle.

Based on the definition of the fatigue crack density, e.g., Eq. (3), the cracked volume of the asphalt binder sample could be calculated with Eq. (22).

$$V_{C,N} = \phi_N V_0, \tag{22}$$

where ϕ_N is the fatigue crack density at the Nth loading cycle, and V_0 is the total volume of the asphalt binder DSR sample.

Then, substituting Eq. (20) to Eq. (22) into Eq. (19) gave

$$\frac{\mathrm{d}\phi}{\mathrm{d}N} = A\left(\frac{W_{R3,N}}{V_0 \dfrac{\mathrm{d}\phi}{\mathrm{d}N}}\right)^n. \tag{23}$$

Rearranging Eq. (23) produced

$$\frac{\mathrm{d}\phi}{\mathrm{d}N} = A^{\frac{1}{n+1}} V_0^{-\frac{n}{n+1}} \left(W_{R3,N}\right)^{\frac{n}{n+1}}. \tag{24}$$

Taking the logarithm of both sides of Eq. (24) yielded

$$\ln\left(\frac{\mathrm{d}\phi}{\mathrm{d}N}\right) = \frac{1}{n+1}\ln A - \frac{n}{n+1}\ln V_0 + \frac{n}{n+1}\ln\left(\frac{1}{2}\tau_{0F}^2\left(\frac{1}{G_{NF}^*} - \frac{1}{G_{VE}^*}\right)\cdot \pi h \cdot \left(\triangle c^2 + 2 r_E \triangle c\right)\right). \tag{25}$$

According to the plot, the fatigue crack density growth rate, and the dissipated pseudo stain energy for cracks in double logarithm scales, the parameters of the modified Paris' law, n and A, were determined with Eq. (26) and Eq. (27), respectively.

$$K = \frac{n}{n+1} \Rightarrow n = \frac{K}{1-K} \tag{26}$$

$$b = \frac{1}{n+1}\ln A - \frac{n}{n+1}\ln V_0 \Rightarrow \ln A = \mathrm{n}\left(b + \ln V_0\right) + b, \tag{27}$$

where K and b are the slope and the intercept of the fitting line of the relationship between the fatigue crack density growth rate and the dissipated stain energy for cracking in double logarithm scales, respectively.

4. Results and discussions

4.1. Crack initiation analysis

To employ the crack initiation criterion of an asphalt binder based on the SFE and RPSE, the SFE components of these two asphalt binders were first calculated using Eq. (1) and Eq. (2) according to the contact angles results of the Wilhelmy plate tests, which are detailed in Table 4. The total SFE and the Lewis polar acid-base component of the SBS modified asphalt binder were

slightly larger than those of the #70 asphalt binder, but the result of the Lifshitz-van der Waals component was the complete opposite.

Table 4 SFE components of binders at 20°C (mJ/m^2).

Asphalt binder	Γ^{LW}	Γ^{+}	Γ^{-}	Γ^{AB}	Γ
#70	13.56	0.98	1.21	2.18	15.74
SBS	11.69	4.06	1.18	4.38	16.07

Once the total SFE of the asphalt binders was determined, the horizontal length of the crack initiation (a) could be calculated using Eq. (12). Additionally, the secant method mentioned in section 3.1 was used to determine the crack length of Stage I (C_0) and the loading cycles corresponding to the C_0. Therefore, the data for the C_0, the loading cycles of Stage I and a were presented in Table 5. It can be seen from Table 5 that the values of C_0 and a both increased with the increasing stress level, and the value of a was far smaller than that of C_0. However, the loading cycles to initiation decreased with the increase of the stress level, which indicated that the higher stress level accelerated the process of crack initiation, resulting in a larger crack length for Stage I. At the beginning of Stage I, the numerous micro cracks occur and these cracks form the circumferential crack. The larger loading cycles within the Stage I means that the asphalt binder shows better capability of crack initiation resistance. Under the lower stress levels, the SBS modifier plays an important role in crack resistance of circumferential crack reformation. When the stress level increases to a certain extent, the SBS may lose the strong ability of crack resistance. Therefore, the loading cycles in Stage I show different attenuation trend under the lower and higher stress levels. Furthermore, the SBS modified asphalt binder showed a larger crack size at the end of Stage I and loading cycles is larger than that of unmodified asphalt at any stress level, which meant that the SBS modifier hindered the crack initiation of the modified asphalt binder compared with the unmodified asphalt binder. As shown in Eq. (12), the calculation of "a" relates the dynamic shear modulus in the linear viscoelastic stage (G_{VE}^{*}), reference modulus (G_R), crack length of Stage I (c_0) and surface free energy (Γ). Herein, G_{VE}^{*} equals to G_R. The value of G_{VE}^{*} and Γ of these two types of asphalt is almost the same. Therefore, the calculation of "a" is dependently determined on value of $\left(r_0 - c_0\right)^2$. As shown in Table 5, the c_0 of SBS modified asphalt is larger than that of unmodified asphalt. Therefore, the SBS modified asphalt exhibits larger crack size in crack initiation. The larger crack size in crack initiation means that the loading cycles within the Stage I is larger and crack density will lingeringly step into the steady growth

383 stage showing crack initiation resistance.

384 **Table 5 Results related to Stage I: C_0, loading cycles and a.**

Asphalt binder	Stress level/ kPa	C_0/mm	CV /%	Cycles of Stage I	CV /%	a/ μm	CV /%
#70	180	0.26	2.21	507	13.2	2.05	3.2
	200	0.29	12.1	495	10.0	2.08	10.2
	220	0.36	4.2	490	12.3	2.16	6.3
	240	0.38	7.4	390	10.9	2.19	7.8
	260	0.45	7.3	370	2.5	2.28	6.5
	280	0.46	0.2	365	1.94	2.29	2.5
	300	0.49	13.2	337	8.5	2.32	10.7
SBS	180	0.44	0.6	885	10.7	3.04	1.1
	200	0.46	13.4	826	15.3	3.06	10.8
	220	0.47	11.1	715	3.0	3.08	9.5
	240	0.53	3.4	535	5.1	3.20	4.7
	260	0.63	2.9	415	5.3	3.39	3.1
	280	0.64	7.7	385	11.0	3.41	6.9
	300	0.74	0.9	355	13.8	3.62	1.8

385 *4.2. Relationship between the fatigue crack density and the DPSE for cracking*

386 Fig. 5(a) shows the relationship between the fatigue crack density (ϕ) and the DPSE for
387 the fatigue crack (W_{R3}) during the entirety of the fatigue testing. At the beginning of testing, there
388 was an approximatively linear relationship between these two parameters. However, when the
389 asphalt binder lost the fatigue crack resistance ability, e.g., stepping into the unstable growth stage
390 (Stage III) mentioned in the section 3.1, the unit growth in the fatigue crack density needed more
391 DPSE, leading to the structural failure of the asphalt binder sample. In particular, the parameters
392 within Stage II followed a linear relationship, as shown in the dashed box. The #70 unmodified
393 asphalt binder as an example, the relationships between the ϕ and W_{R3} at 5 stress levels within
394 Stage II are shown in Fig. 5(b). This meant that the unit DPSE caused an equal amount of increase
395 in the fatigue crack density, which potently demonstrated that the secant method was a
396 considerably effective way to determine the range of the steady growth stage (Stage II) from the
397 view of the DPSE.

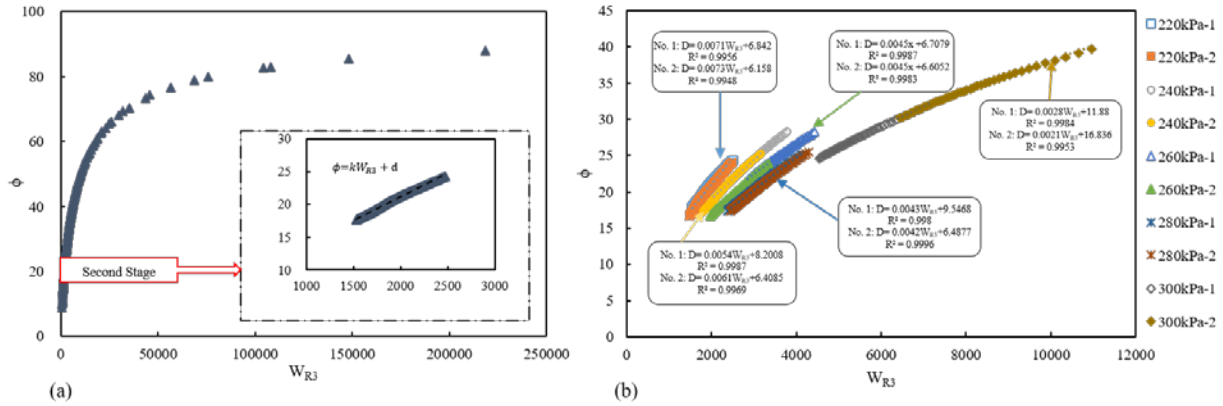

Fig. 5 Relationship between the fatigue crack density and DPSE for the fatigue crack: (a) during the entirety of the fatigue testing and (b) the parameters of #70 unmodified asphalt binder at 5 stress levels (220 kPa, 240 kPa, 260 kPa, 280 kPa, and 300 kPa) within Stage II.

Table 6 The slope of the linear formulation between the fatigue crack density and W_{R3}.

Asphalt binder	Stress level/ kPa	Slop (k)					
		No. 1	R^2	No. 2	R^2	Average	CV /%
#70	180	0.0144	0.9960	0.0139	0.9950	0.0143	1.7
	200	0.0101	0.9924	0.0095	0.9963	0.0098	3.1
	220	0.0071	0.9956	0.0073	0.9948	0.0072	1.4
	240	0.0054	0.9987	0.0061	0.9969	0.0058	6.0
	260	0.0045	0.9987	0.0045	0.9983	0.0045	0.0
	280	0.0043	0.9980	0.0042	0.9996	0.0043	1.2
	300	0.0028	0.9984	0.0021	0.9953	0.0025	14.0
SBS	180	0.0070	0.9914	0.0073	0.9929	0.0072	2.1
	200	0.0083	0.9966	0.0073	0.9964	0.0078	6.4
	220	0.0040	0.9905	0.0048	0.9914	0.0044	9.1
	240	0.0029	0.9828	0.0029	0.9859	0.0029	0.0
	260	0.0022	0.9871	0.0024	0.9902	0.0023	4.3
	280	0.0018	0.9850	0.0023	0.9922	0.0021	11.9
	300	0.0013	0.9876	0.0012	0.9814	0.0013	3.8

Based on the analysis above, Table 6 shows the slope of the linear formulation (e.g., the parameter k shown in the Fig. 5(a)) between the fatigue crack density and W_{R3} within the second stage of the #70 unmodified asphalt binder and the SBS modified asphalt binder for different stress levels. It was clearly seen from the table that there was a linear relationship between these two parameters because of the high R^2 values (>0.98). In general, the value of the slope decreased with the increase of stress levels, which meant that the same incremental fatigue crack density would generate a larger dissipation of energy for the higher stress level. Therefore, the loading cycles of Stage II would decrease with the increasing stress level.

4.3. Modified Paris' law coefficients A and n

Based on the testing data of the time sweep tests, Eq. (25), which was established using the modified Paris' law, was applied to determine the coefficients n and A. Table 7 details the values of the coefficients n and A, which were shown in the logarithm form of the #70 unmodified asphalt binder and the SBS modified asphalt binder under various stress levels. It could be found from Table 7 that the values of log(A) and n were approximatively constant within a significantly larger stress level range regardless of the #70 unmodified asphalt binder or the SBS modified asphalt binder. The average values of log(A) containing 14 calculated data points for the #70 unmodified asphalt binder and the SBS modified asphalt binder were -8.04 and -5.28, respectively. Likewise, those of n for the two asphalt binders were 2.57 and 1.17. Meanwhile, the corresponding variable coefficients (CVs) of the four groups of data were 9.83%, 9.30%, 13.05%, and 13.52%, respectively. The analysis showed that the coefficients n and A are independent on stress levels. Compared with the unmodified asphalt binder, the SBS modified asphalt binder had a larger value of log(A) and a smaller value of n, which meant that the fatigue crack density evolution speed of the SBS modified asphalt binder was slower than that of unmodified asphalt binder. In other words, the SBS modified asphalt binder possessed better fatigue crack resistance ability. The SBS was a copolymer that consisted of rigid polystyrene (PS) blocks and rubbery polybutadiene (PB) blocks. The blocks showed a cross-linked elastomer network [41]. Therefore, the network played an important role in hindering the extension of the fatigue crack. Fig. 6 presents the morphology of SBS polymer in the modified asphalt binder obtained by laser scanning confocal microscope (LSCM) using the 488-nm laser diode, where the fluorescence phase is SBS-rich and the darker phase is bitumen-rich. As shown in Fig 6, the SBS phase uniformly lies in the modified asphalt binder. The continuous SBS polymer phase improves the mechanical property of asphalt binder with respect to crack resistance, and this is the reason why the SBS modified asphalt binder shows better ability of crack resistance compared with the unmodified asphalt binder.

Another finding from Table 7 was that there was an excellent linear relationship between the values of log(A) and that of n, which were fitted using a linear model, as shown in Fig. 7. The high R^2 value demonstrated that either log(A) or n was suitable for evaluating the fatigue crack resistance of asphalt binders. There were some related findings from other papers [8, 27, 39], as shown in Fig. 8. Luo et al.'s analysis [39] verified a strong correlation between the two parameters of different asphalt mixtures according to the test data from Jacobs's [42] dynamic uniaxial tensile

test, Luo et al.'s [25] controlled-strain RDT test, and Gu et al.'s [43] overlay test, which is shown in Fig. 8(a). Luo et al. [27] developed a theoretical model through rigorous derivation to characterize the linear relationship between the Paris' law coefficients A and n of four types of asphalt mixtures, as shown in Fig. 8(b). Furthermore, the results of the Paris' law parameters of the unmodified asphalt binder and the modified asphalt binder from Li et al. [8] are displayed in Fig. 8(c). No matter what type of research object (asphalt binder or asphalt mixture) was studied, or what kind of law (Paris' law or modified Paris' law) was used for analysis, the coefficients n and A in the logarithmic form were always highly correlated with each other. Moreover, the coefficient n was an excellent indicator, compared with coefficient A, for evaluating the crack resistance of asphalt materials, which was proven using sensitivity analysis by examining the damage density behaviors in response to the changes of two coefficients [25]. Generally, the material with a smaller value of n showed better fatigue crack resistance performance.

As analyzed in section 4.1, the higher stress level would cause a larger horizontal length for the crack initiation (a). However, the coefficients A and n that were used to model the fatigue crack density evolution did not show obvious changes with the increasing stress level.

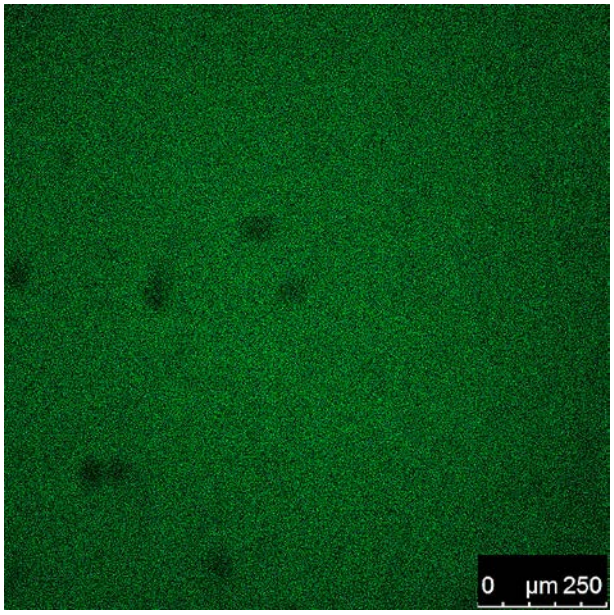

Fig. 6 Fluorescence image of SBS modified asphalt taken by laser scanning confocal microscope (LSCM).

Table 7 Modified Paris' law coefficients under different stress levels.

Asphalt binder	Stress level/ kPa	No.	log(A)	n	Asphalt binder	Stress level/ kPa	No.	log(A)	n
#70	180	1	-8.45	2.88	SBS	180	1	-5.88	1.33
		2	-7.86	2.84			2	-5.79	1.40
	200	1	-8.46	2.91		200	1	-5.57	1.30
		2	-7.45	2.37			2	-5.68	1.14
	220	1	-6.98	2.18		220	1	-5.68	1.29
		2	-8.87	2.78			2	-5.67	1.25
	240	1	-8.90	2.78		240	1	-4.87	1.01
		2	-9.05	2.98			2	-4.46	0.84
	260	1	-8.24	2.46		260	1	-5.73	1.31
		2	-7.56	2.63			2	-4.96	1.07
	280	1	-9.11	2.81		280	1	-5.17	1.17
		2	-7.14	2.13			2	-5.07	1.19
	300	1	-7.61	2.24		300	1	-4.49	0.96
		2	-6.85	1.98			2	-4.90	1.16

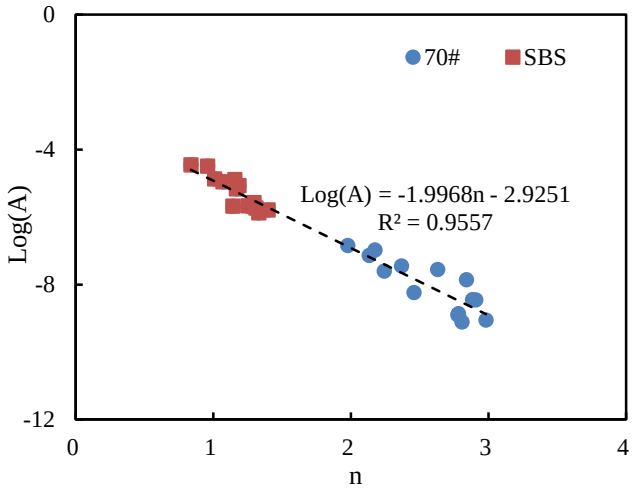

Fig. 7 Relationship between the modified Paris' law coefficients.

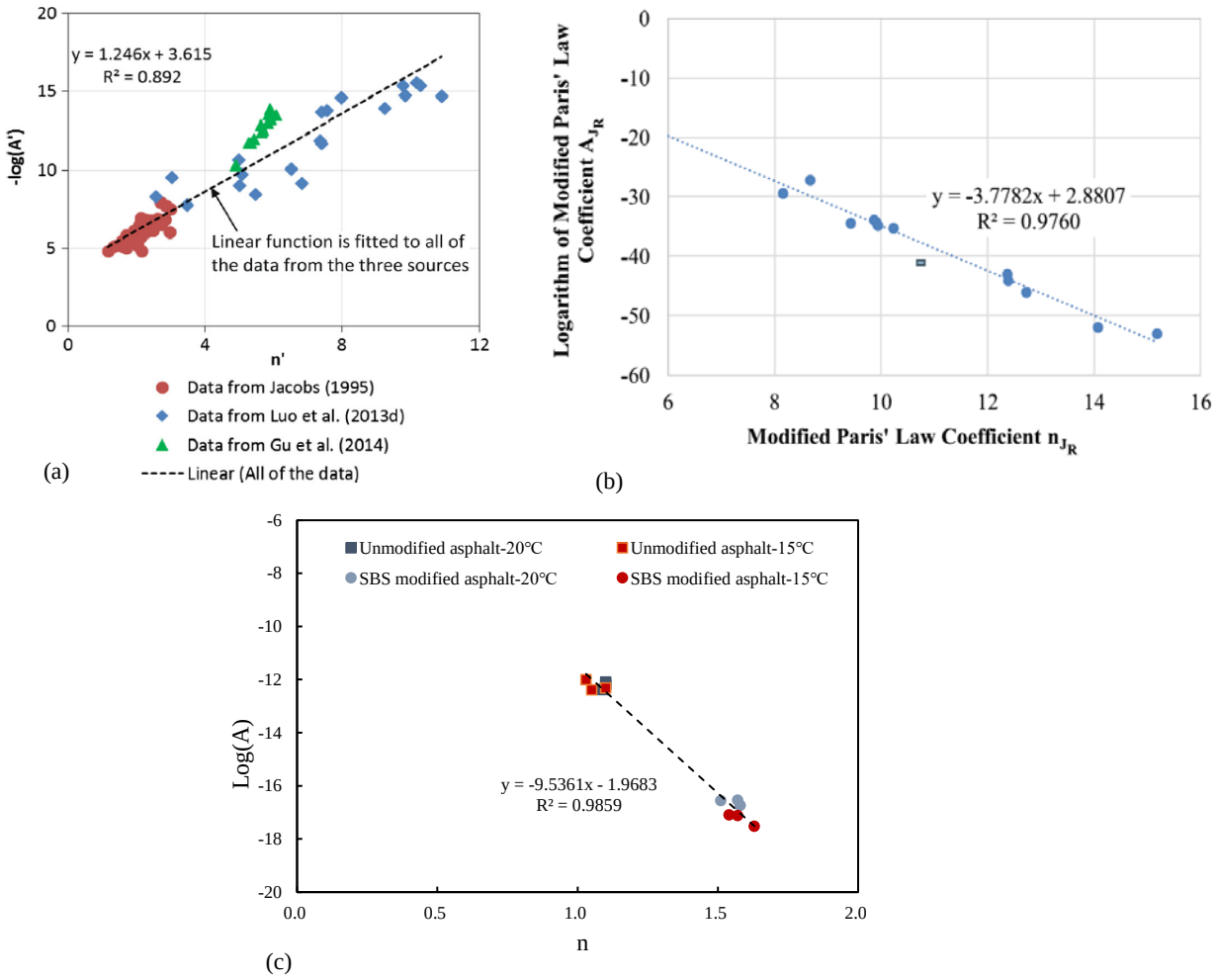

Fig. 8 Analysis of relationship between those two coefficients from previous literatures. (a) analysis of Luo et al. [39] based on the data from Jacobs [42], Luo et al. [25] and Gu et al. [43]; (b) analysis of Luo et al. [27] and (c) data from Li et al. [8].

5. Summary and conclusions

Targeting the analysis of fatigue crack density evolution within the steady growth stage of two types of asphalt binders, the crack initiation and the propagation were characterized based on the Griffith theory and the modified Paris' law, respectively. The main findings and conclusions are summarized as follows:

1. The horizontal lengths of the crack initiation for two asphalt binders increased with the increasing stress level.
2. The SBS modified asphalt binder showed better crack initiation resistance because of a larger value of the crack length in Stage I and the crack initiation and loading cycles to initiation

at any stress level. This was due to the SBS modifier hindering the crack initiation of the modified asphalt binder compared with the unmodified asphalt binder.

3. The total DPSE generation during the fatigue process contained three parts: (1) viscoelastic energy, (2) DPSE for permanent deformation, and (3) DPSE for cracking. When the test temperature was 20°C, the main damage to the asphalt binder was a fatigue crack. The fatigue crack density and the DPSE for cracking within the steady growth stage followed a linear relationship. Their fitting results demonstrated that the secant method is a considerably effective method for determining the range of the steady growth stage.

4. The fatigue crack density growth rate was modeled with a modified Paris' law by only considering the DPSE for cracking, and the coefficients A and n were determined.

5. Those two parameters, e.g., n and Log(A), were almost identical under various stress levels, which meant that they were inherent to the material performance. Additionally, there was a linear relationship between n and Log(A).

6. A smaller value of n indicated that the asphalt binder showed an excellent fatigue crack resistance. Therefore, the SBS modified asphalt binder possesses a better fatigue crack resistance ability because of the cross-linked elastomer network in the modified asphalt binder.

Declaration of interests

The authors declare that they have no known competing financial interests or personal relationships that could have appeared to influence the work reported in this paper.

Acknowledgments

The authors acknowledge the financial support of the National Natural Science Foundation of China (No. 51778140, No. 52078130), Technology Research and Development Program of China State Railway Group Co., Ltd (P2019G030) and the Scientific Research Foundation of Graduate School of Southeast University (YBPY2158).

References

[1]C. Hintz, and H. Bahia. Understanding mechanisms leading to asphalt binder fatigue in the dynamic shear rheometer. *Road Materials and Pavement Design*, 2013. 14: 231-251. doi:10.1080/14680629.2013.818818

[2]H. Chen, Y. Zhang, and H. U. Bahia. The role of binders in mixture cracking resistance measured by ideal-ct test. *International Journal of Fatigue*, 2021. 142. doi:10.1016/j.ijfatigue.2020.105947

[3]H. Chen, and H. Bahia. Modelling effects of aging on asphalt binder fatigue using complex modulus and the las test. *International Journal of Fatigue*, 2021. 146. doi:10.1016/j.ijfatigue.2021.106150

[4]Y. Q. Tan, L. Y. Shan, Y. R. Kim, and B. S. Underwood. Healing characteristics of asphalt binder. *Construction and Building Materials*, 2012. 27(1): 570-577. doi:10.1016/j.conbuildmat.2011.07.006

[5]L. Y. Shan, S. Tian, H. S. He, and N. Q. Ren. Internal crack growth of asphalt binders during shear fatigue process. *Fuel*, 2017. 189: 293-300. doi:10.1016/j.fuel.2016.10.094

[6]C. Wang, Y. F. Chen, and L. H. Song. Investigating the crack initiation and propagation of asphalt binder in linear amplitude sweep test. *Journal of Materials in Civil Engineering*, 2020. 32(12). doi:10.1061/(asce)mt.1943-5533.0003470

[7]Y. Zhang, and Y. Gao. Predicting crack growth in viscoelastic bitumen under a rotational shear fatigue load. *Road Materials and Pavement Design*, 2019. doi:10.1080/14680629.2019.1635516

[8]H. Li, X. Luo, W. Yan, and Y. Zhang. Energy-based mechanistic approach for crack growth characterization of asphalt binder. *Mechanics of Materials*, 2020. 148. doi:10.1016/j.mechmat.2020.103462

[9]C. Shi, X. Cai, X. Yi, T. Wang, and J. Yang. Fatigue crack density of asphalt binders under controlled-stress rotational shear load testing. *Construction and Building Materials*, 2021. 272. doi:10.1016/j.conbuildmat.2020.121899

[10]L. U. Shan, Y. Q. Tan, S. Underwood, and Y. R. Kim. Application of thixotropy to analyze fatigue and healing characteristics of asphalt binder. *Transportation Research Record*, 2010. (2179): 85-92. doi:10.3141/2179-10

[11]R. Jahangir, D. Little, and A. Bhasin. Evolution of asphalt binder microstructure due to tensile loading determined using afm and image analysis techniques. *International Journal of Pavement Engineering*, 2015. 16(4): 337-349. doi:10.1080/10298436.2014.942863

[12]R. H. Doremus. Cracks and energy—criteria for brittle fracture. *Journal of Applied Physics*, 1976. 47(5): 1833-1836. doi:10.1063/1.322901

[13]Y. Gao, L. Li, and Y. Zhang. Modelling crack initiation in bituminous binders under a rotational shear fatigue load. *International Journal of Fatigue*, 2020. 139. doi:10.1016/j.ijfatigue.2020.105738

[14]X. Luo, R. Luo, and R. L. Lytton. Energy-based crack initiation criterion for viscoelastoplastic materials with distributed cracks. *Journal of Engineering Mechanics*, 2015. 141(2). doi:10.1061/(asce)em.1943-7889.0000830

[15]W. G. Knauss. Stable and unstable crack growth in viscoelastic media. *Journal of Rheology*, 1969. 13(3): 291-313. doi:Transactions of the Society of Rheology

[16]R. A. Schapery. A theory of crack initiation and growth in viscoelastic media. *International Journal of Fracture*, 1975. 11(1): 141-159. doi:10.1007/bf00034721

[17]Y. Q. Zhang, X. Luo, R. Luo, and R. L. Lytton. Crack initiation in asphalt mixtures under external compressive loads. *Construction and Building Materials*, 2014. 72: 94-103. doi:10.1016/j.conbuildmat.2014.09.009
[18]L. Li, Y. Gao, and Y. Zhang. Fatigue cracking characterisations of waste-derived bitumen based on crack length. *International Journal of Fatigue*, 2021. 142.
[19]E. Arambula, E. Masad, and A. E. Martin. Moisture susceptibility of asphalt mixtures with known field performance - evaluated with dynamic analysis and crack growth model. *Transportation Research Record*, 2007. (2001): 20-28. doi:10.3141/2001-03
[20]E. Masad, V. T. F. C. Branco, D. N. Little, and R. Lytton. A unified method for the analysis of controlled-strain and controlled-stress fatigue testing. *International Journal of Pavement Engineering*, 2008. 9(4): 233-246. doi:10.1080/10298430701551219
[21]F. J. Zhou, P. Karki, and S. Im. Development of a simple fatigue cracking test for asphalt binders. *Transportation Research Record*, 2017. (2632): 79-87. doi:10.3141/2632-09
[22]Y. M. Gao, L. L. Li, and Y. Q. Zhang. Modeling crack propagation in bituminous binders under a rotational shear fatigue load using pseudo j-integral paris' law. *Transportation Research Record*, 2020. 2674(1): 94-103. doi:10.1177/0361198119899151
[23]L. Li, Y. Gao, and Y. Zhang. Crack length based healing characterisation of bitumen at different levels of cracking damage. *Journal of Cleaner Production*, 2020. 258. doi:10.1016/j.jclepro.2020.120709
[24]Z. M. Si, D. N. Little, and R. L. Lytton. Characterization of microdamage and healing of asphalt concrete mixtures. *Journal of Materials in Civil Engineering*, 2002. 14(6): 461-470. doi:10.1061/(asce)0899-1561(2002)14:6(461)
[25]X. Luo, R. Luo, and R. L. Lytton. Modified paris's law to predict entire crack growth in asphalt mixtures. *Transportation Research Record*, 2013. (2373): 54-62. doi:10.3141/2373-06
[26]Y. Q. Zhang, R. Luo, and R. L. Lytton. Mechanistic modeling of fracture in asphalt mixtures under compressive loading. *Journal of Materials in Civil Engineering*, 2013. 25(9): 1189-1197. doi:10.1061/(asce)mt.1943-5533.0000667
[27]R. Luo, and H. Chen. An improved method of characterizing fracture resistance of asphalt mixtures using modified paris' law: Part ii-establishment of index for fracture resistance. *Mechanics of Materials*, 2019. 138. doi:10.1016/j.mechmat.2019.103168
[28]R. Luo, and H. Chen. Improved method of characterizing fracture resistance of asphalt mixtures using modified paris' law: Development of methodology. *Journal of Materials in Civil Engineering*, 2020. 32(10). doi:10.1061/(asce)mt.1943-5533.0003357
[29]R. A. Schapery. Correspondence principles and a generalized j integral for large deformation and fracture analysis of viscoelastic media. *International Journal of Fracture*, 1984. 25(3): 195-223. doi:10.1007/bf01140837
[30]M. T. China. (2011). Standard test methods of bitumen and bituminous mixtures for highway engineering. In. Beijing: China Communications Press.
[31]M. o. T. o. China. (2004). Technical specification for construction of highway asphalt pavements In. Beijing: China Communications Press.
[32]Z. Zeng, B. S. Underwood, and C. Castorena. Low-temperature performance grade characterisation of asphalt binder using the dynamic shear rheometer. *International Journal of Pavement Engineering*, 2020. doi:10.1080/10298436.2020.1774766
[33]R. Luo, D. Zhang, Z. Zeng, and R. L. Lytton. Effect of surface tension on the measurement of surface energy components of asphalt binders using the wilhelmy plate method. *Construction and Building Materials*, 2015. 98: 900-909.

doi:10.1016/j.conbuildmat.2015.08.125
[34]D. Zhang, and R. Luo. Using the surface free energy (sfe) method to investigate the effects of additives on moisture susceptibility of asphalt mixtures. *International Journal of Adhesion and Adhesives*, 2019. 95. doi:10.1016/j.ijadhadh.2019.102437
[35]C. J. Vanoss, M. K. Chaudhury, and R. J. Good. Interfacial lifshitz-van der waals and polar interactions in macroscopic systems. *Chemical Reviews*, 1988. 88(6): 927-941. doi:10.1021/cr00088a006
[36]T. M. Ahmed. Fatigue performance of hot mix asphalt tested in controlled stress mode using dynamic shear rheometer. *International Journal of Pavement Engineering*, 2019. 20(3): 255-265. doi:10.1080/10298436.2016.1172707
[37]X. Luo, R. Luo, and R. L. Lytton. Energy-based mechanistic approach to characterize crack growth of asphalt mixtures. *Journal of Materials in Civil Engineering*, 2013. 25(9): 1198-1208. doi:10.1061/(asce)mt.1943-5533.0000666
[38]E. Masad, V. T. F. C. Branco, D. N. L. Lytton, and R. A unified method for the analysis of controlled-strain and controlled-stress fatigue testing. *International Journal of Pavement Engineering*, 2008.
[39]X. Luo, Y. Q. Zhang, and R. L. Lytton. Implementation of pseudo j-integral based paris' law for fatigue cracking in asphalt mixtures and pavements. *Materials and Structures*, 2016. 49(9): 3713-3732. doi:10.1617/s11527-015-0750-z
[40]P. C. Paris, and F. Erdogan. A critical analysis of crack propagation laws. *Journal of Basic Engineering*, 1963. 85(4): 528–533.
[41]C. D. Qian, W. Y. Fan, G. M. Yang, L. Han, B. D. Xing, and X. B. Lv. Influence of crumb rubber particle size and sbs structure on properties of cr/sbs composite modified asphalt. *Construction and Building Materials*, 2020. 235. doi:10.1016/j.conbuildmat.2019.117517
[42]M. Jacobs. (1995). *Crack growth in asphaltic mixes.* The Delft University of Technology, The Netherlands.
[43]F. Gu, Y. Q. Zhang, X. Luo, R. Luo, and R. L. Lytton. Improved methodology to evaluate fracture properties of warm-mix asphalt using overlay test. *Transportation Research Record*, 2015. (2506): 8-18. doi:10.3141/2506-02